Taylor & Francis
Taylor & Francis Group

Thermo-Mechanical Wave Propagations in Shape Memory Alloy Rod with Phase Transformations

L. X. Wang

University of Southern Denmark, Sonderborg, Denmark

R. V. N. Melnik

University of Southern Denmark, Sonderborg, Denmark, and Wilfrid Laurier University, Waterloo, ON, Canada

In the present study, a mathematical model is developed to analyze the wave propagation processes in shape memory alloy rods. The first order phase transformations and associated thermo-mechanical coupling effects are accounted for by employing the modified Ginzburg-Landau-Devonshire theory. The effect of internal friction is considered by using a Rayleigh dissipation term. Chebyshev collocation method is employed together with the backward differentiation methods for numerical analysis. Numerical experiments are performed. Wave propagations caused by impact loadings are analyzed for different initial temperatures. It is demonstrated that thermal waves will be induced. Phase transformations in the material will complicate their propagation patterns. Dissipation effects are enhanced by internal friction, while dispersion during wave propagations is induced by interfacial energy term.

1. INTRODUCTION

In the past decades, different aspects of Shape Memory Alloys (SMA) have been investigated intensively by mathematicians, physicists, and engineers [1]. This interest in a larger scientific community is due to SMA unique properties of being able to convert thermal energy into mechanical and vice versa. These properties are promising for many applications of SMAs, including mechanical and control engineering, biomedicine, communication, robotics to name just a few [1]. Motivated by application developments of advance composite materials involving SMAs, nonlinear wave propagations in these materials have been investigated as a stepping ground for the prediction and understanding of dynamic response of the composite under various dynamic loadings [2–4].

Compared to wave propagations in conventional solid materials, the impact induced wave propagations in materials such as SMAs require delicate treatment as additional difficulties arise due to phase transformations [5–7]. In general, impact loadings of these materials will cause nonlinear thermo-mechanical waves which are similar to those of other thermo-elastic materials under impact loadings. The difference of wave propagation in conventional solids and those in the ferroelastic materials such as SMAs is that the first order martensitic transformation may be induced in the latter case. The transformation is reversible, and its native nonlinearity and hysteresis will have a substantial influence on the wave propagation and will make the wave propagation patterns more complicated [5, 7, 8].

The first step to the modelling of impact induced wave propagations and phase transformations is a sound constitutive theory upon which the entire model can be built [2, 4, 8]. Various constitutive models have been proposed on mesoscale and microscale to capture the phase boundary movement induced by the dynamical loadings [9, 10]. Examples of such a constitutive model can be found in [2, 9] where an one-dimensional model for the modelling of shock wave propagations with phase transformation was constructed on the basis of a non-convex Helmholtz free energy function. Under this approach the entire structure was split into different domains due to the phase transformation and the movement of boundaries between the domains was modelled using the "jump conditions." This approach is suitable for microscopic problems, while for many engineering applications a model is required at macroscale. In [11, 12], the dynamic behavior of phase boundaries was modelled using a thermo-mechanical coupling approach. The model was based on a linearized constitutive theory, and hence its application potential was inherently limited.

For many engineering applications, the dynamic response of SMA materials caused by impact loadings needs to be better understood at macroscale for design and control of SMA-based devices. For this purpose, displacement and temperature evolutions in the material are normally sought. Models at mesoscale

may not be sufficient for this purpose as another model needs to be constructed to link macroscale properties and mesoscale domain structures. Another aspect of modelling the dynamics of such materials as SMAs under impact loadings is the thermo-mechanical coupling effects. In most of the existing investigations, the thermal dynamics are either neglected [2, 3, 10], or modelled separately from the mechanical dynamics [11, 12]. However, the physics-based models should account for the intrinsic coupling of thermal and mechanical fields in SMAs. When the SMAs are used for damping purposes or for other purposes where the conversion of energy between the thermal and mechanical fields is essential, the coupling effects are expected to be particularly important, and the constitutive theory should be constructed by taking into account both fields simultaneously.

In this paper, the nonlinear thermo-mechanical wave propagations in SMA rods induced by impact loadings are modelled and analyzed at macroscale. To capture the thermo-mechanical coupling and nonlinear nature of the phase transformations, the Ginzburg-Landau-Devonshire theory is applied for the modelling of the nonlinear dynamics. The governing equations for the mechanical field are obtained by minimizing the mechanical energy, while those for the thermal field are obtained by using the conservation law of internal energy. The intrinsic coupling of the two fields is built-in into the model by including both fields in the potential energy functional. In the following sections, a mathematical model describing SMA dynamics is developed based on a system of coupled partial differential equations which is re-cast in the form of differential algebraic equations, and Chebyshev collocation method is employed together with the backward differentiation formula to integrate the resulting system. Nonlinear wave propagation patterns caused by an impact stress loading at one end of the rod are simulated with different initial temperatures and computational parameters. Finally, the influence of phase transformation on the wave propagations is analyzed numerically, along with the influence of other effects such as internal friction and capillary effects.

2. THE INITIAL-BOUNDARY VALUE PROBLEM

We restrict our analysis to one-dimensional cases as sketched in Figure 1. The SMA rod under consideration occupies an interval $[0, L]$, and is subjected to an impact loading from the right end $x = L$, while the other end $x = 0$ is fixed. The rod is thermally insulated at both ends so there is no heat loss (gain) to (from) the ambient environment. Under external loadings, a material point x in the SMA rod will be moved to a new position $x + u(x, t)$ due to deformation, where $u(x, t)$ is the longitudinal
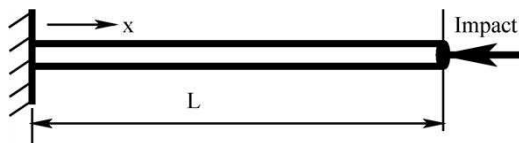

FIG. 1.   Shape memory alloy rod under impact loadings.

displacement at time t. Function $u(x, t)$ is assumed to be continuous at any time t and position x based on the continuity of the rod at macroscale. The stress σ is related to the deformation ε by $\sigma(x, t) = \mathcal{N}(\varepsilon(x, t))$ where $\varepsilon(x, t) = \partial u(x, t)/\partial x$ is the strain, while $\mathcal{N}(\varepsilon(x, t))$ is a nonlinear function to be determined for characterization of the material properties.

By now, it is well understood that the first order phase transformation (during which both stable and meso-stable phases may occur) in SMAs holds the key to unique properties of the material, such as the shape memory and pseudo-elastic effects. Therefore, it is expected that the adequate mathematical model for the dynamics of SMAs at macroscale should be capable of capturing the first order martensite phase transformations. On the other hand, the intrinsic coupling of mechanical and thermal fields should also be captured by the model. To satisfy these requirements, the mathematical model based on the modified Ginzburg-Landau-Devonshire theory has been established [4, 13, 14]:

$$\rho\ddot{u} = \frac{\partial(}{\partial x}k_1(\theta - \theta_1)\varepsilon + k_2\varepsilon^3 + k_3\varepsilon^5)$$

$$+\nu\frac{\partial}{\partial t}\frac{\partial^2 u}{\partial x^2} - k_g\frac{\partial^4 u}{\partial x^4} + f, \tag{1}$$

$$c_v\frac{\partial\theta}{\partial t} = k\frac{\partial^2\theta}{\partial x^2} + k_1\theta\varepsilon\frac{\partial\varepsilon}{\partial t} + \nu(\frac{\partial\varepsilon}{\partial t})^2 + g, \tag{2}$$

where k_1, k_2, k_3 and k_g are material-specific constants, ν internal friction coefficient, ρ the density of the material, θ_1 the reference temperature, c_v the specific heat capacitance, k heat conductance, and f and g mechanical and thermal loadings, respectively.

It is essential that the above model is constructed on the basis of the potential energy function $\mathcal{F}$, which is a non-convex function of the chosen *order parameters* and temperature θ, at mesoscale, according to Ginzburg-Landau-Devonshire theory. It is a sum of local energy function ($\mathcal{F}_l$) and non-local energy function ($\mathcal{F}_g$). For the current one-dimensional problem, the strain $\varepsilon(x, t)$ is chosen as the order parameter, and the local free energy density can be constructed as the Landau free energy density $\mathcal{F}_l(\theta, \varepsilon)$, while the non-local part can be formulated as a Ginzburg term $\mathcal{F}_g(\nabla\varepsilon)$ [4, 15, 16]:

$$\mathcal{F}(\theta, \varepsilon) = \mathcal{F}_l(\theta, \varepsilon) + \mathcal{F}_g(\nabla\varepsilon),$$

$$\mathcal{F}_l(\theta, \varepsilon) = \frac{k_1(\theta - \theta_1)}{2}\varepsilon^2 + \frac{k_2}{4}\varepsilon^4 + \frac{k_3}{6}\varepsilon^6, \tag{3}$$

$$\mathcal{F}_g(\nabla\varepsilon) = \frac{1}{2}k_g\left(\frac{\partial\varepsilon}{\partial x}\right)^2,$$

The local minima of the local term (Landau free energy function) are introduced to characterize martensite variants, while the non-local term (Ginzburg term) above accounts for inhomogeneous strain field, which represents energy contributions from domain walls and other boundaries among different phases. It will be translated into capillary effects at macroscale.

In order to account for the internal friction, accompanying wave propagations and phase transformations, which will be translated into viscous effects at macroscale, a Rayleigh dissipation term is also included in the above model by using the following term [9]:

$$\mathcal{F}_R = \frac{1}{2}\nu\left(\frac{\partial \varepsilon}{\partial t}\right)^2. \quad (4)$$

The constitutive relations for the material in the above model at macroscale can be obtained by using the thermodynamic equilibrium conditions:

$$\sigma = \frac{\partial H}{\partial \varepsilon}, \quad e = \mathcal{H} - \theta\frac{\partial \mathcal{H}}{\partial \theta}. \quad (5)$$

where $\mathcal{H}(\theta, \varepsilon) = \mathcal{F} - c_v\theta\ln\theta$ is the Helmholtz free energy function. The mechanical and thermal fields are intrinsically coupled since the internal energy e is associated with the same potential energy as above, and the governing equations for the thermal field are formulated using the conservation law for the internal energy [4,13].

The difficulties associated with the above model are understood better by analyzing the profiles of the non-convex potential energy F_l, its temperature dependence, and the non-convex constitutive curves, as sketched in Figure 2. The coefficient values used for this illustration is the same as those given in section 5. At low temperature $\theta = 210$ K, as sketched in the top row, there are two local minima in the potential function, which are introduced to characterize martensite plus and minus, respectively (in 1D cases). The stress-strain relation of the material under dynamical loadings will not follow the sketched constitutive relations exactly. Instead, there will be jumps from point (A to B) or vice versa. Such jumps are associated with the transition from martensite plus to minus or vice versa. This is the origin of mechanical hysteresis which will dissipate mechanical energy quickly by converting it into thermal form due to the thermo-mechanical coupling. The amount of energy converted into thermal form can be estimated by using the area enclosed under the hysteresis loop, as marked by the dashed lines in the stress-strain plot on the left. When the SMA rod temperature is intermediate ($\theta = 240$ K), there are still hysteresis loops, and the jump phenomena become more complicated, since there are three local minima present in the potential energy function, which means that austenite and two martensite variants may co-exist in the material. The dissipation of mechanical energy will be slower in this case since the hysteresis loop becomes smaller. At high temperature ($\theta = 310$ K), it is shown that there are no jump phenomena any longer, therefore no hysteresis, because there is only one local minimum. In this case, there will be only austenite present and the dynamics become fairly simple.

In the current paper, the mechanical loading is implemented in terms of impact stress at one of the rod ends. Hence, it is convenient to keep the constitutive relation as an extra equation for the model and consider the stress as a dependent variable. This representation will make the treatment of boundary conditions much easier for the current discussion. The resulting system of Differential Algebraic Equations (DAE) can be written as follows [7]:

$$\frac{\partial u}{\partial t} = v, \quad \rho\frac{\partial v}{\partial t} = \frac{\partial \sigma}{\partial x} + \nu\frac{\partial}{\partial x}\frac{\partial v}{\partial x} - k_g\frac{\partial}{\partial x}\frac{\partial^2 \varepsilon}{\partial x^2},$$
$$c_v\frac{\partial \theta}{\partial t} = k\frac{\partial^2 \theta}{\partial x^2} + k_1\theta\varepsilon\frac{\partial \varepsilon}{\partial t}, \quad (6)$$
$$\sigma = k_1(\theta - \theta_1)\varepsilon + k_2\varepsilon^3 + k_3\varepsilon^5,$$

where v is the velocity. The mechanical and thermal loadings, f and g, are all set to zero, so that only boundary loadings will be taken into account in the current investigation.

In order to investigate the thermo-mechanical wave propagations in the SMA rod, the following boundary conditions are employed for the mechanical and thermal fields similarly as in [13, 18]:

$$\left.\frac{\partial \theta}{\partial x}\right|_{x=0} = 0, \quad \left.\frac{\partial \theta}{\partial x}\right|_{x=L} = 0,$$
$$u(0, t) = 0, \quad \sigma(L, t) = S(t), \quad (7)$$
$$\left.\frac{\partial^2 u}{\partial x^2}\right|_{x=0} = 0, \quad \left.\frac{\partial^2 u}{\partial x^2}\right|_{x=L} = 0. \quad (8)$$

where $S(t)$ is a given function describing the stress impact profile.

3. WAVE PROPAGATIONS

Since mechanical responses caused by external loadings in most materials are normally much faster than thermal ones, which are also more interesting for numerical investigations and many applications, the emphasis of the current discussion is put on mechanical waves caused by mechanical loadings.

3.1. Temperature Dependence

For the analysis of elastic waves in the SMA rod, Eq. (1) is firstly linearized at the point (σ_L, ε_L) where $\sigma_L = 0$:

$$\rho\ddot{u} = \frac{\partial}{\partial x}k_L\varepsilon + \nu\frac{\partial}{\partial t}\frac{\partial \varepsilon}{\partial x} - k_g\frac{\partial^4 u}{\partial x^4}, \quad (9)$$

where the external mechanical loading is dropped out. k_L is the stiffness constant for the linearized system, which is temperature dependent.

When the SMA is at high temperature ($\theta = 310$ K), only austenite is stable and there is no phase transformation, it can be easily calculated that $\varepsilon_L = 0$ so k_L can be simply formulated as: $k_L = k_1(\theta - \theta_1)$.

At lower temperature ($\theta = 210$ K), the stress strain relation is not a monotone curve any longer, and the linearization has to be carried out by using at least three points, as indicated by the plot in the top row of Figure 2 (the three intersections
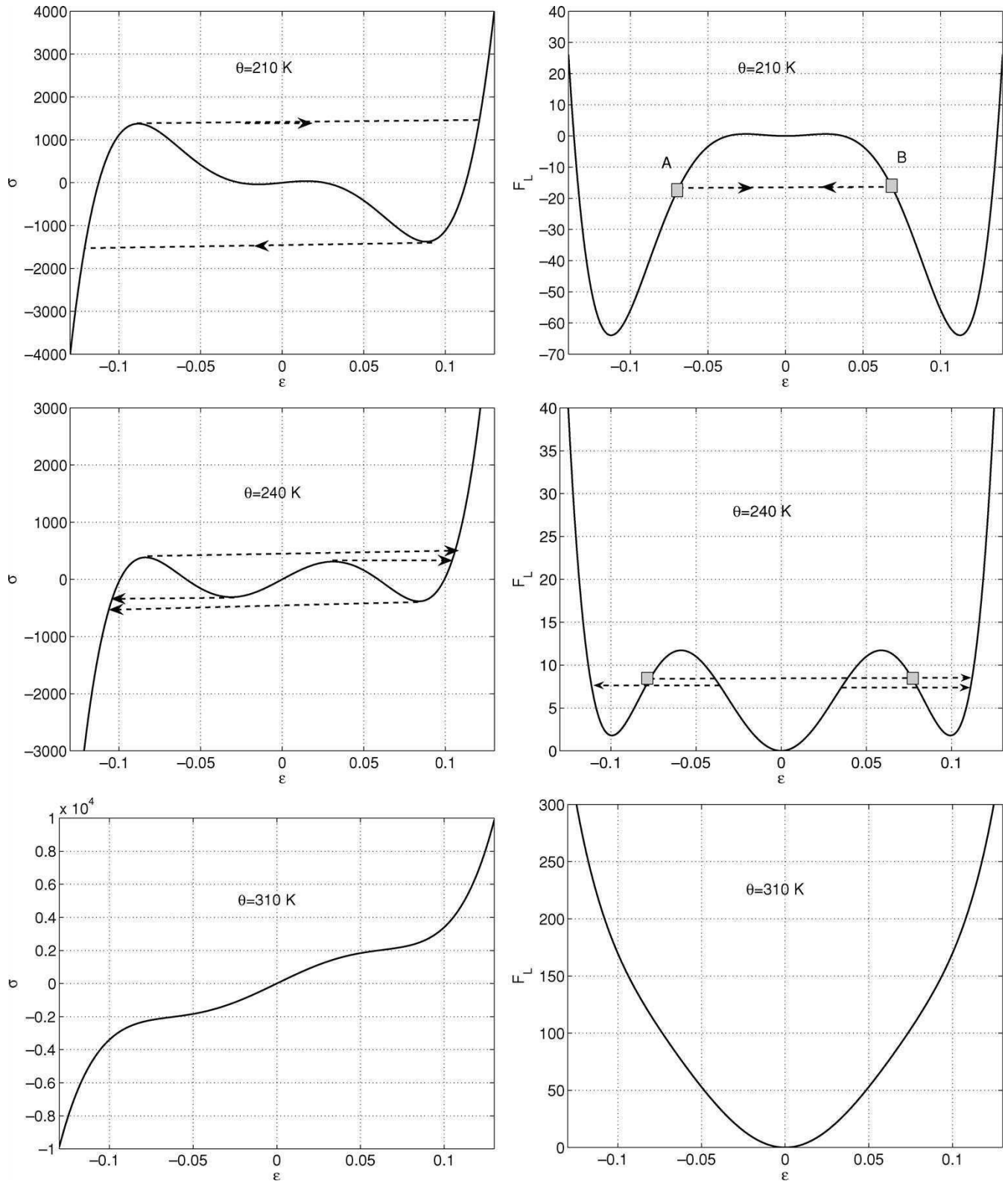
FIG. 2. Constitutive relations (left column) for a shape memory alloy and the associated potential energy density (right column), at various temperatures. (top) θ = 210 K. (middle) θ = 240 K. (bottom) θ = 310 K.

between the horizontal axis with the $\sigma - \varepsilon$ curve). The central one is $\varepsilon_L = 0$, which is not a stable equilibrium state of the system, and is not interesting for the analysis. The other two intersections can be easily calculated using the following condition:

$$k_1(\theta - \theta_1) + k_2\varepsilon^2 + k_3\varepsilon^4 = 0, \tag{10}$$

which gives the following formulation (using parameter values given in section 5):

$$\varepsilon_L^2 = \frac{-k_2 \pm \sqrt{k_2^2 - 4k_1k_3(\theta - \theta_1)}}{2k_3}, \quad \varepsilon_L = \pm 0.115. \tag{11}$$

These two values are associated with strains for martensite plus ($\varepsilon_L = 0.115$) and minus ($\varepsilon_L = -0.115$), respectively. The linearized coefficient then can be calculated as follow:

$$k_L = k_1(\theta - \theta_1) + k_2\varepsilon_L^2 + k_3\varepsilon_L^4, \tag{12}$$

which gives k_L the same value at the two points with different ε_L values, due to the symmetry property. The above analysis indicates that the linearized wave motion in the material at martensite plus state will be the same as those at martensite minus state.

For the cases where the SMA rod temperature is intermediate, the dependence of k_L on temperature is more complicated since both austenite and martensite might occur and there might be 4 values for ε_L to satisfy $\sigma_L = 0$, as indicated in the middle row in Figure 2. Although the symmetry property still exists for martensitic variants, wave motions are different between austenite and martensite states.

Let us consider the following wave solution to the linearized wave motion given by Eq. (9):

$$u = u(x - Vt) = u(z), \quad z = x - Vt, \tag{13}$$

where V is a constant stands for wave velocity. By substitution, the following relation can be easily obtained:

$$k_g \frac{\partial^2 \varepsilon}{\partial x^2} = (k_L - \rho V^2)\varepsilon - \nu V \frac{\partial \varepsilon}{\partial x}, \tag{14}$$

where $k_L - \rho V^2$ can be positive or negative. The problem is now formulated as an ordinary differential equation and its general solution can be written as:

$$\varepsilon(z) = (C_1 + C_2 z)e^{z\sqrt{(k_L - \rho V^2)/k_g}}, \tag{15}$$

where C_1, C_2 are coefficients to be determined by boundary conditions. The viscous term is temporarily ignored.

If the wave velocity V is less than the velocity of sound in the material $V_s = \sqrt{k_L/\rho}$, then $k_L - \rho V^2 > 0$, and there is no limited solution, since the exponential function has a positive index and will becomes infinity. It means that no waves can propagate in the material with velocity V smaller than the velocity of sound in the material. Since the velocity of sound of the material is temperature dependent, so the allowed speed for waves to propagate in the SMA rod varies along with the variation of its temperature.

When the viscous term is also taken into account, then the wave propagation will always be accompanied by dissipation effects, which can be characterized by the following exponential function:

$$|\varepsilon(z)| = e^{-\xi\omega z}, \quad \xi = \frac{\nu V}{2\sqrt{(\rho V^2 - k_L)k_g}},$$
$$\omega = \sqrt{\frac{(\rho V^2 - k_L)}{k_g}}, \tag{16}$$

where the initial amplitude of the considered waves are assume to be 1. The dissipation effects can be estimated by the exponential coefficient $\xi\omega = \frac{\nu V}{2k_g}$. For larger V, faster dissipation will be induced. The dissipation effects are independent of the material temperature.

3.2. Effects of Ginzburg's Term

In the wave equation, the term $k_g \frac{\partial^4 u}{\partial x^4}$ is resulted from the interfacial energy contribution to the potential energy function. It is also called Ginzburg's term, and accounts for the capillary effects [4, 13, 14, 20]. It is easy to see that this term is related to dispersion of wave propagations. For the analysis, the following solution to the linearized wave equation is considered:

$$u = \sin \frac{2\pi}{\lambda}(x - Vt), \tag{17}$$

where λ is the wave length. By substitution, the following relationship involves the wave speed V can be obtained if the viscous effects are ignored:

$$\rho V^2 = k_L + \frac{4\pi k_g}{\lambda^2}, \tag{18}$$

which indicates that the wave propagation speeds are increased due to the contribution of non-local potential energy (capillary effects). The dispersion effects caused by non-local contributions are stronger for those waves with smaller wave lengths. If the SMA rod is at lower temperature, the linearized stiffness constant k_L will be smaller, which will make the last term in Eq. (18) more pronounced.

4. NUMERICAL METHODOLOGY

As mentioned in the previous section, the development of the numerical methodology for simulation of the wave propagation based on the above mathematical model is not a trivial task. In particular, given that both dispersion and dissipation of wave propagations are present in the physics of the problem, the numerical algorithm for the problem has to be able to take care of

both dissipation and dispersion numerically, and the accuracy of the algorithm will be affected by their treatment. In the present paper, a multi-domain decomposition method combined with the Chebyshev collocation methodology is the method of choice in addressing the above issues. The compromise made here is that a spectral method is employed to take advantage of its better convergence property, while the domain decomposition method is chosen to reduce the order of basis functions for the spectral method when the total node number is large.

4.1. Chebyshev Collocation Method

For the Chebyshev pseudo-spectral approximation, a set of Chebyshev points $\{x_i\}$ are chosen along the length direction as follows:

$$x_i = L\left(1 - \cos\left(\frac{\pi i}{N}\right)\right)\Big/2, \quad i = 1, 2, \ldots, N. \quad (19)$$

Using these nodes, u, v, θ, and σ distributions in the rod can be expressed in terms of the following linear approximation:

$$f(x) = \sum_{i=1}^{N} f_i \phi_i(x), \quad (20)$$

where $f(x)$ stands for any of u, v, θ, or σ, and f_i is the function value at x_i. $\phi_i(x)$ is the ith interpolating polynomial which has the following property:

$$\phi_i(x_j) = \begin{cases} 1, & i = j, \\ 0, & i \neq j. \end{cases} \quad (21)$$

It is easy to see that the well-known Lagrange interpolants satisfy the interpolating requirements. Having obtained $f(x)$ approximately, the derivative $\partial f(x)/\partial x$ can be easily obtained by taking the derivative of the basis functions $\phi_i(x)$ with respect to x:

$$\frac{\partial f}{\partial x} = \sum_{i=1}^{N} f_i \frac{\partial \phi_i(x)}{\partial x}, \quad (22)$$

and similarly for the higher order derivatives. All these approximations can be formulated in the matrix form, for the convenience of programming.

4.2. Multi-Domain Decomposition

It is known that the spectral methods are able to give a higher accuracy with the same number of discretization nodes, compared to finite difference methods or finite element methods. On the other hand, when the solution to the problem does not have higher-order derivatives, the spectral methods may lead to artificial oscillations due to the Gibbs phenomenon. This may be expected for the current problem when the impact induced wave propagation is analyzed numerically. To avoid this, a multi-domain decomposition method is employed.
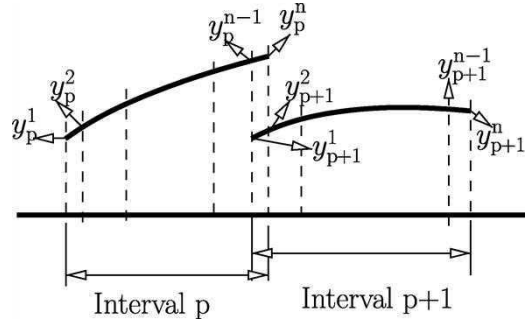

FIG. 3.   Sketch of domain decomposition and discretization.

The entire computational domain $\mathcal{D} = [0, L]$ is evenly decomposed into P intervals (subdomains), with an overlap region between each pair of consecutive intervals, as sketched in Figure 3:

$$\mathcal{D} = \bigcup_{p=1}^{p=P} D_p, \quad (23)$$

where the number of subdomains P is chosen according to the specific problem under consideration. In each interval, the Chebyshev collocation method discussed in the previous section is employed to approximate the solution and its derivatives.

The coupling between each pair of consecutive intervals can be implemented by setting the following requirements:

$$y_p^n = y_{p+1}^2, \quad y_p^{n-1} = y_{p+1}^1, \quad (24)$$

where the subscript p stands for the interval number, while the superscript n stands for the node number in each interval. Variable y_p^n is the function value at point x_p^n (the nth node in the pth interval), which could be any of the dependent variables we are solving for. Point x_p^n is actually the same node as x_{p+1}^2, and x_p^{n-1} is the same node as x_{p+1}^1.

The derivatives of functions in the overlapped nodes are approximated by taking the average of their values evaluated from the two intervals involved:

$$\frac{\partial y}{\partial x}\bigg|_{x_p^{n-1}} = \frac{1}{2}\left(\sum_{i=0}^{N} y_p^i \frac{\partial \phi_i(x)}{\partial x}\bigg|_{x_p^{n-1}} + \sum_{i=0}^{N} y_{p+1}^i \frac{\partial \phi_i(x)}{\partial x}\bigg|_{x_{p+1}^1}\right), (25)$$

$$\frac{\partial y}{\partial x}\bigg|_{x_p^n} = \frac{1}{2}\left(\sum_{i=0}^{N} y_p^i \frac{\partial \phi_i(x)}{\partial x}\bigg|_{x_p^n} + \sum_{i=0}^{N} y_{p+1}^i \frac{\partial \phi_i(x)}{\partial x}\bigg|_{x_{p+1}^2}\right).$$

The approximation to the second order derivatives can be found using the same average for the nodes in the overlapped region. By using the above average, it is clear that there will be no jumps of approximated $\frac{\partial y}{\partial x}$ in the overlapped region caused by the approximation using domain decomposition.

4.3. Backward Differentiation Formula Method

By employing the multi-domain decomposition methods combined with the Chebyshev collocation methodology, the given set of partial differential equations Eq. (6) can be converted into ordinary differential equations. While the last row in Eq. (6) (the last row gives the $\sigma \sim \varepsilon$ relation) is also discretized using Chebyshev collocation methods, which will yield a set of algebraic equations. By combining the ordinary differential equations and algebraic equations together, the whole system can be generically written in the following form:

$$M\frac{dX}{dt} + N(t, X, g(t)) = 0, \tag{26}$$

where X is the vector collecting all the variables we are solving for, M is a singular matrix, since all those rows assigned for algebraic equations are zero. N is a vector collecting nonlinear functions produced by spatial discretization. The resultant DAE system is a stiff system and has to be solved by an implicit algorithm. Here the second order backward differentiation formula method is employed for this purpose. By discretizing the time derivative using the second order backward approximation, the DAE system can be converted into an algebraic system at each time level, which can formally written as follows:

$$M\left(\frac{3}{2}X^n - 2X^{n-1} + \frac{1}{2}X^{n-2}\right) + \Delta t\,N(t_n, X^n, g(t_n)) = 0, \tag{27}$$

where n denotes the current computational time layer. For each computational time layer, iterations must be carried out using Newton's method for X^n by use of X^{n-1} and X^{n-2}. Starting from the initial value, the vector of unknowns X can be solved for at all specified time instances employing this algorithm. The stop criterion for the iteration is that the relative residual is smaller than $1e^{-6}$. The details for the numerical algorithm can be found in [20].

5. NUMERICAL EXPERIMENTS

A series of numerical experiments have been carried out to investigate the nonlinear wave propagations in the SMA rod involving phase transformations. All experiments reported here have been performed on a $Au_{23}Cu_{30}Zn_{47}$ rod, with a length of 1 cm. The physical parameters, except ν and k_g, for this specific material are taken the same as those in [20, 21], which are listed as follows for convenience:

$k_1 = 480\,\mathrm{g/(ms^2 cm\,K)}, \quad k_2 = 6 \times 10^6 \mathrm{g/(ms^2 cm\,K)},$

$k_3 = 4.5 \times 10^8\,\mathrm{g/(ms^2 cm\,K)},$

$\theta_1 = 208\,\mathrm{K}, \quad \rho = 11.1\,\mathrm{g/cm^3}, \quad c_v = 3.1274\,\mathrm{g/(ms^2 cm\,K)},$

$k = 1.9 \times 10^{-2}\,\mathrm{cm\,g/(ms^3 K)}.$

Experiments indicate that the Ginzburg coefficient k_g should be relatively small compared to k_1, so it is taken as $k_g =$ 10 $\mathrm{g/ms^2}$ first, by referring to [7]. The internal friction coefficient is not an easily measurable quantity. In what follows, we assume it to be a small fraction (2%) of k_1, that is approximately 10 $\mathrm{g/((cm)(ms))}$. The entire rod is divided into 10 sub-intervals, in each interval there are 15 nodes used for spatial discretization. All simulations have been carried out for the time span [0, 0.1] ms, and the time step-size for the integration is chosen as 2.5×10^{-5} ms.

The first numerical experiment for nonlinear wave propagations in the SMA rod is performed with a higher temperature $\theta = 310$ K, for which there is no phase transformation. Other initial conditions are chosen $u = v = \sigma = 0$, and mechanical loading is employed in terms of a stress impact at right end, as follows:

$$g(t) = \begin{cases} 4 \times 10^3, & 0 \le t \le 0.005\ \mathrm{ms} \\ 0, & t > 0.005\ \mathrm{ms} \end{cases} \tag{28}$$

which can be regarded as an approximation to a pulse stress impact on the SMA rod.

The mechanical wave propagations are presented by the strain evolution while thermal waves by temperature evolution in Figure 4. It is shown that the impact induced waves start from $x = 1$ and propagate along the negative x direction, hit the opposite boundary at $x = 0$ and are bounced back. The temperature evolution indicates that there are associated thermal waves induced by the stress impact loading, due to the thermo-mechanical coupling effects. The propagation patterns of the thermal waves are similar to those of mechanical waves. The evolution of the displacement distribution due to the stress impact is also presented in Figure 4, in the left bottom sub-figure. To clarify the patterns of wave propagations, the strain distributions in the SMA rod at three chosen time instants are plotted in the right bottom sub-figure in Figure 4 ($t = 0.01, 0.02, 0.03$ ms, respectively). The arrow attached to each wave profile is to indicate its propagation direction. It is seen that the strain distributions in the SMA rod are always smooth and no obvious sharp jump occurs, since only austenite is stable with this temperature and there is no phase transformation. The amplitude of the wave decreases and the wave peak becomes broader during the propagation, which can be easily explained by the fact that dissipation effects and dispersion effects, caused by internal friction, capillary effects, and thermo-mechanical coupling, are all included in the model. The average wave propagation speed can be estimated by the location of the wave frontier or wave peak plotted in the figure. With the current initial temperature, the strain wave is bounced back from $x = 0$ and its peak is located around $x = 0.65$ cm when $t = 0.03$ ms. This experiment simulates the nonlinear thermo-mechanical waves like those in regular thermo-elastic materials.

The second example deals with the same computational conditions and loading, except that the initial temperature now is set $\theta = 240$ K, for which both martensite and austenite may co-exist in the SMA rod. The numerical results for this case are
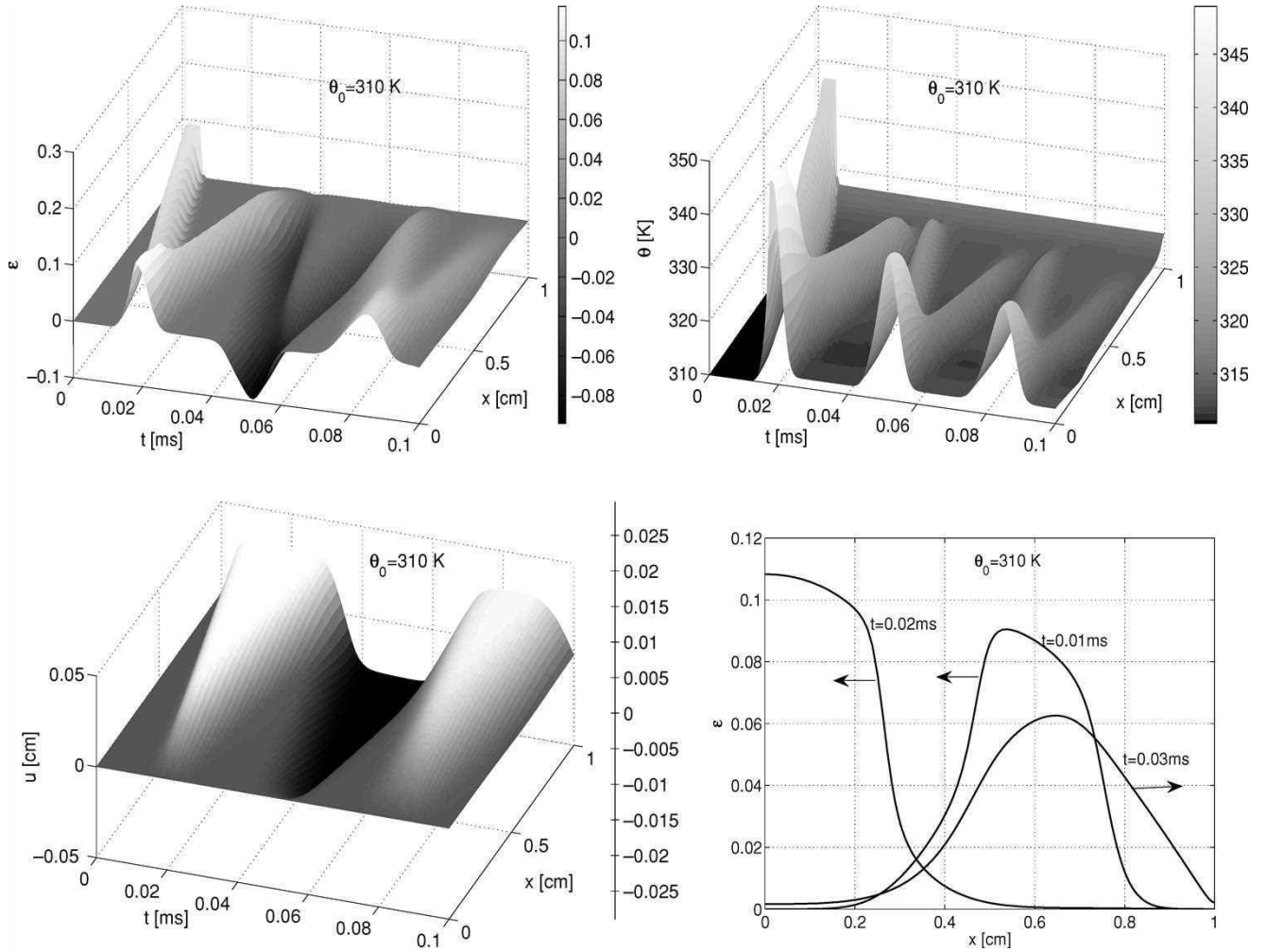
FIG. 4.   Nonlinear thermo-mechanical wave propagations in a shape memory alloy rod caused by a stress impact, initial temperature is $\theta = 310$ K.

presented similarly in Figure 5. It is easy to see that the strain and temperature waves are not as regular as those in the first experiment. There are some plateaus clearly shown in the strain and temperature figures, which can be related to martensite and austenite in the SMA rod. The frontier of the waves are now more easily identified since abrupt jumps occur in the strain distribution, which are caused by phase transformations between austenite and martensite. In the displacement evolution now we have only one peak within the simulated time span, while two peaks are found in the first experiment. On the three chosen time instants, the strain distributions are not as smooth as those at high temperature. At $t = 0.03$ ms, the wave frontier is around $x = 0.65$ cm, propagating along the positive x direction. It indicates that the wave speed is a little lower than that in the first experiment, as indicated by the analysis given in section 3. Similarly, there are thermal waves caused by the mechanical loading due to the coupling effects.

For the third experiment, the initial temperature is set at $\theta = 210$ K. Because only martensite is stable at this temper-

ature, the initial condition is chosen such that the SMA rod is originally at martensite minus state, for which the displacement is set $u = -0.115x$ so $\varepsilon_0 = -0.115$. This strain value is one of the local minima of the non-convex potential energy plotted in Figure 2, and calculated in Eq. (11). Numerical results for this case are presented in Figure 6. It is seen that the entire SMA rod is divided into two domains, one consists of martensite plus (with $\varepsilon \approx 0.115$), and the other one—martensite minus ($\varepsilon \approx -0.115$). The interface between the two domains is driven by the impact stress loading, as sketched in the strain evolution plot and the wave profiles on the chosen time instants in Figure 6. With the given computational conditions, the SMA rod is converted from martensite minus to plus from the end which under impact loading, the phase boundary is driven to propagate along the negative x direction. Due to the hysteretic nature of the phase transformation, the input mechanical energy is dissipated continuously during the propagation of the phase boundary, and is not able to convert the whole rod into martensite plus. The interface stops at around $x = 0.5$. Correspondingly, there are also thermal waves
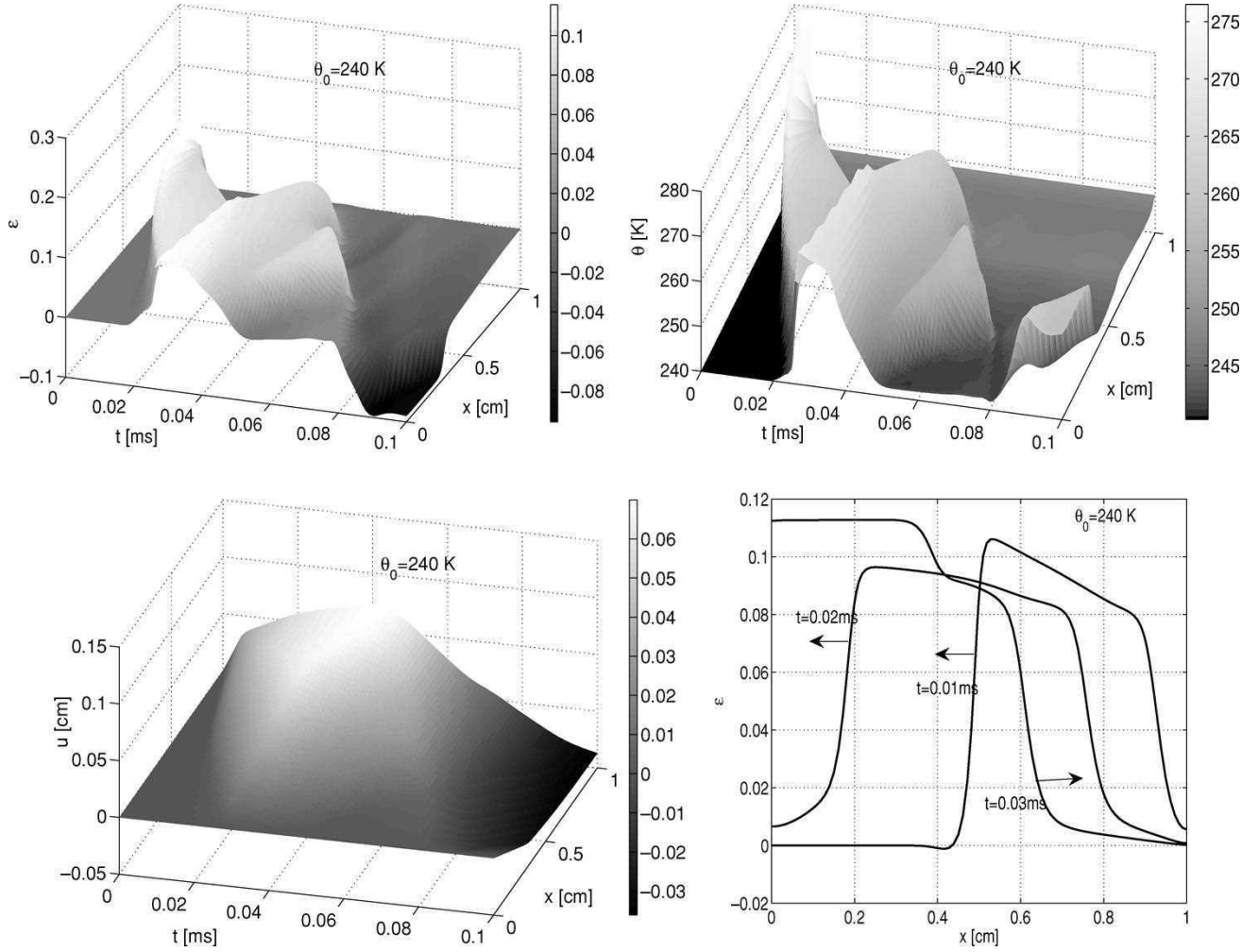
FIG. 5. Nonlinear thermo-mechanical wave propagations involving phase transformations in a shape memory alloy rod caused by a stress impact, initial temperature is $\theta = 240$ K.

accompanying the martensite transformation. The wave propagation speed is much lower compared to those in the previous experiments, and the wave speed changes more remarkably during the propagation process, as indicated by the plot of wave profiles plot at chosen time instants. At $t = 0.03$ ms, the wave frontier is at $x = 0.5$ cm and is unable to move further toward the end $x = 0$.

The fourth experiment is to investigate the dissipation effects due to internal friction in the material. As analyzed in section 3, the dissipation effects are independent of temperature, so we set the initial temperature at $\theta_0 = 310$ K to exclude phase transformation, so that the comparison will be easier. The internal friction ν is set three times larger at 30, and all other computational parameters are chosen the same as those in the first experiment. The strain evolution and wave profiles at the same three chosen time instants are presented in Figure 7. By comparing with those in Figure 4, it is observed that the dissipation effects are enhanced, the peak values of the wave decrease

faster. At $t = 0.01$ ms, the peak value of the wave profile is around 0.075, located around $x = 0.6$ cm, while the counterparts with $\nu = 10$ are peak value 0.089 at around $x = 0.055$ cm. This indicates that when ν is increased, not only the peak value dissipated faster, but the wave speed was also slightly slowed down.

The final experiment is to show numerically the dispersion effects due to the Ginzburg term in the wave equation. As indicated by Eq. (18), the dispersion effects are more pronounced at low temperature since $k_L = k_1(\theta - \theta_1)$ will be smaller. To perform the analysis, the initial conditions are set the same with those in the third experiment, except that k_g is set three times larger at 30. The strain evolution and wave profiles for three chosen time instants are presented in Figure 8. By comparing the results with those in Figure 6, it can be seen that the entire rod is still divided into two domains, one for martensite plus ($\varepsilon \approx 0.115$) and the other—for martensite minus ($\varepsilon \approx -0.115$). However, the wave propagation speed is faster with larger k_g value. The interface
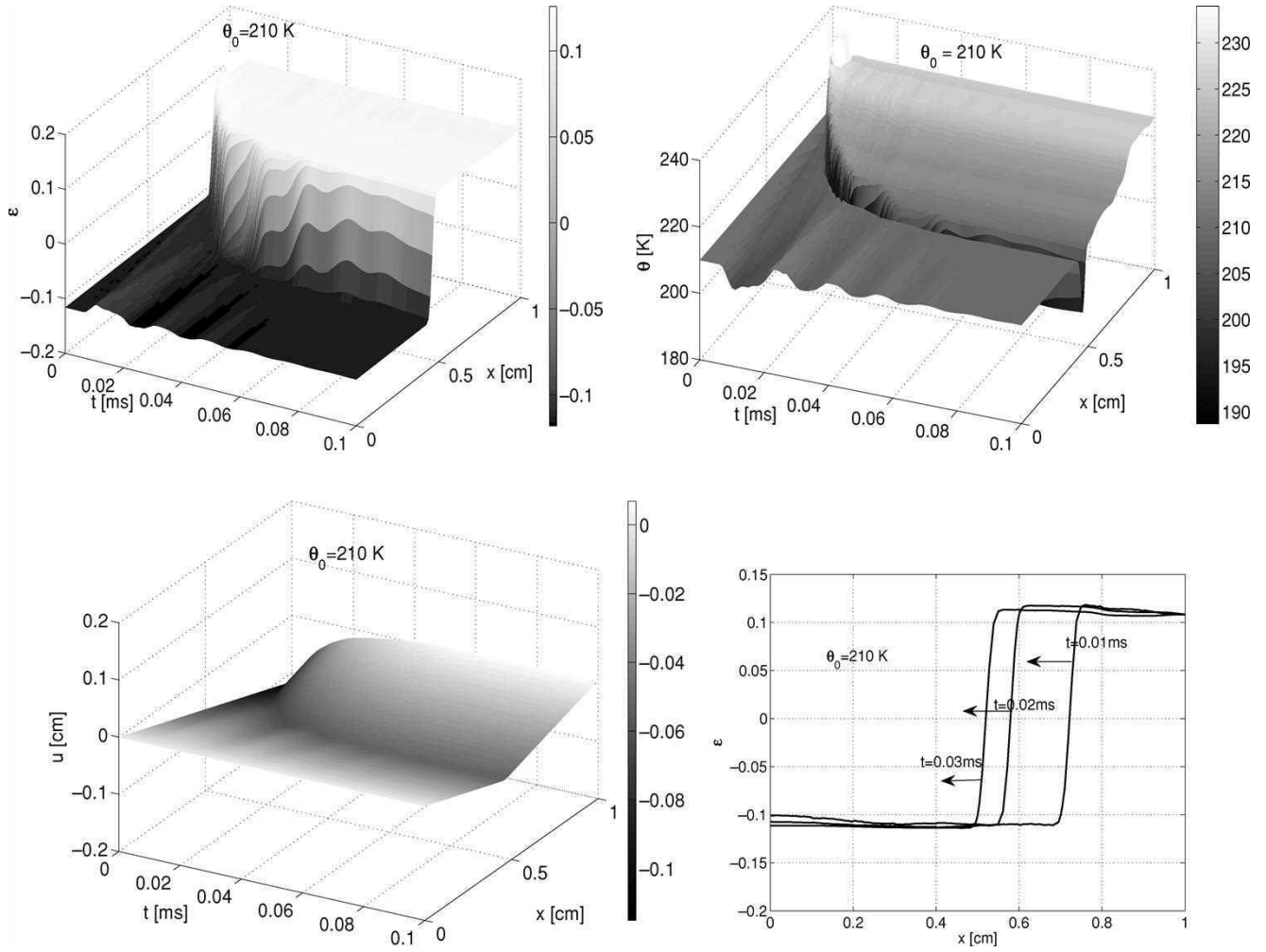
FIG. 6.   Nonlinear thermo-mechanical wave propagation in the shape memory alloy rod caused by a stress impact, involving martensite phase transformations. Initial temperature is $\theta = 210$ K.
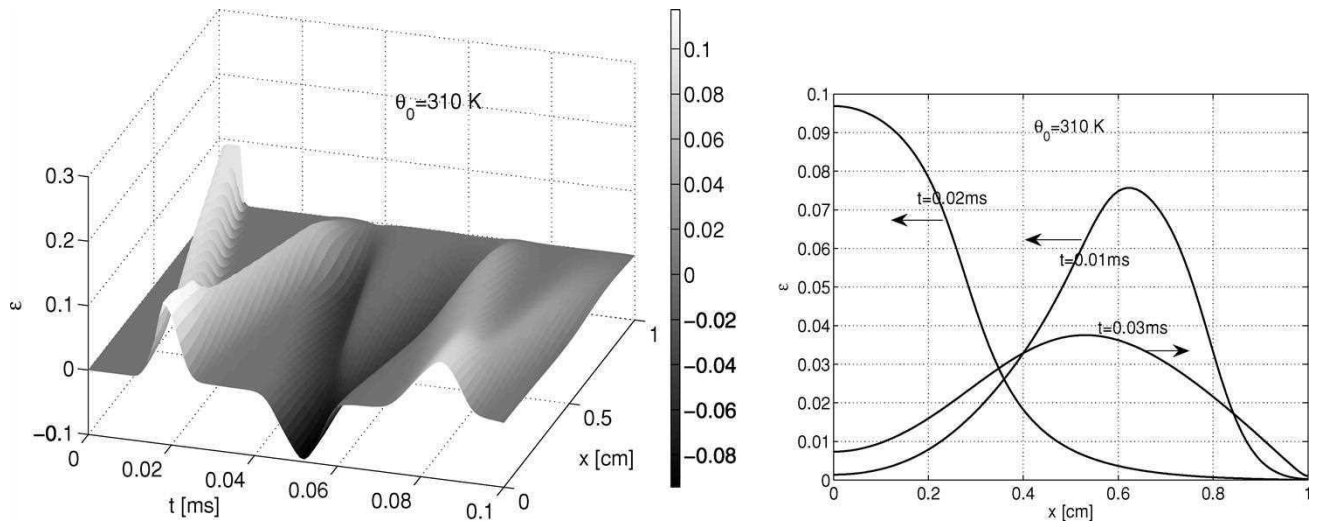

FIG. 7.   Numerical analysis of the dissipation effect of internal friction on wave propagations in a shape memory alloy rod. Initial temperature is $\theta = 310$ K, $\nu = 30$.
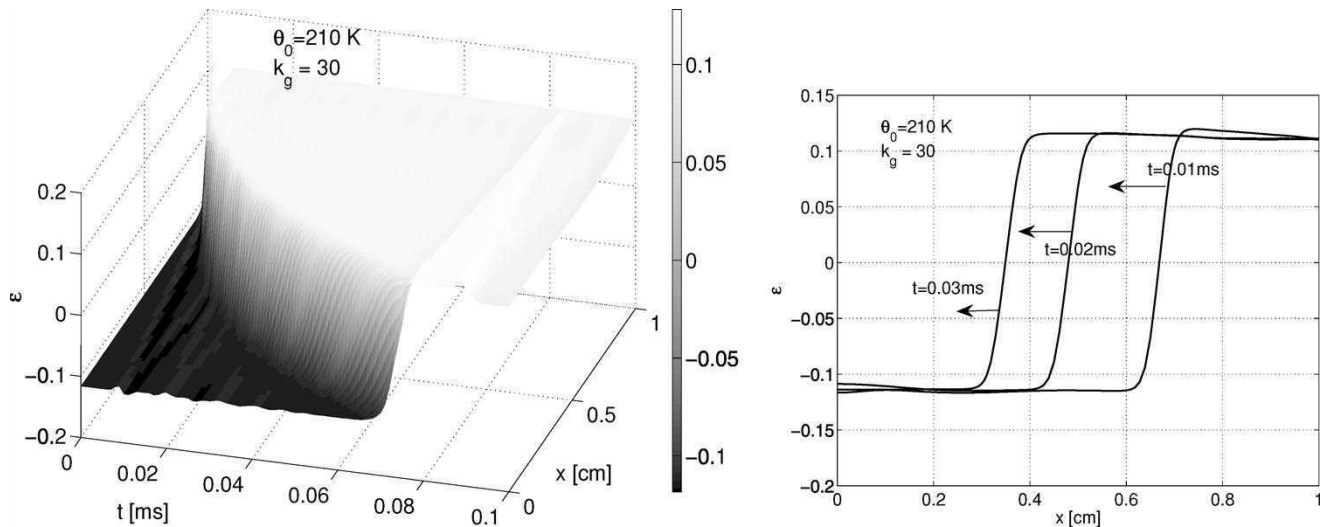
FIG. 8. Numerical analysis of the dispersion effects caused by capillary effects in wave propagations in a shape memory alloy rod. Initial temperature is $\theta = 210$ K, $k_g = 30$.

between martensite minus and plus is located at around $x = 0.35$ cm when $t = 0.03$ ms, while for $k_g = 10$ it is at $x = 0.5$ cm. This observation agrees with the linearization analysis carried out in section 3. At the same time, the entire rod is converted from martensite minus to plus, which indicates that smaller amount of input energy is demanded for the phase transformation when k_g value is larger. In other words, the phase transformation becomes easier to deal with when the capillary effects are enhanced.

From the above numerical experiments follow that nonlinear thermo-mechanical wave propagations caused by impact loadings in the SMA rod can be remarkably influenced by the material temperature, internal friction, and capillary effects. Thermal waves could be induced by impact mechanical loadings. Wave propagation patterns are more complicated when phase transformations are involved, and the dynamic response of the material in this case is very different from those with no phase transformations.

6. CONCLUSIONS

In this paper, a mathematical model for the analysis of wave propagations in a shape memory alloy rod induced by a stress impact was constructed. The modified Ginzburg-Landau-Devonshire theory was employed for modelling dynamic processes in SMA rods. The first order phase transformations and thermo-mechanical coupling were incorporated into the model. A multi-domain decomposition method was employed in conjunction with the Chebyshev collocation method for spatial discretization, and the backward differentiation formula was used for solving the resulting differential-algebraic system. The nonlinear thermo-mechanical wave propagations in the SMA rod were simulated with various initial temperatures (with and without phase transformation). It is shown that wave propagation

pattern at high temperature is more regular, and it was complicated by phase transformation when temperature is low. Remarkable dissipation were observed at low temperature due to phase transformation, it has also has contribution from internal friction. The dispersion effect are more pronounced since the interfacial energy becomes so. The overall wave propagation speed is smaller at low temperature compared to those at higher temperatures.

REFERENCES

1. Birman, V., "Review of mechanics of shape memory alloys structures," *Appl. Mech. Rev.* **50**, 629–645 (1997).
2. Abeyaratne, R., and Knowles, J. K., "Dynamics of propagating phase boundaries: Thermoelastic solids with heat conduction," *Arch. Rational Mech. Anal.* **126**, 203–230 (1994).
3. Berezovski, A., and Maugin, G.A., "Stress-induced phase transition front propagation in thermoelastic solids," *Eur. J. Mech.—A/Solids* **24**, 1–21 (2005).
4. Falk, F., "Ginzburg-Landau theory and solitary wave in shape memory alloys," *Z. Phys. B Condensed Matter* **54**, 159–167 (1984).
5. Bekker, A., Jimenez-Victory, J. C., Popov, P., and Lagoudas, D. C., "Impact Induced propagation of phase transformation in a shape memory alloy rod," *Int. Jour. Plasticity* **18**, 1447–1479 (2002).
6. Dai, X. Y., Tang, Z. P., Xu, S. L., Guo, Y. B., and Wang, W. Q., "Propagation of macroscopic phase boundaries under impact loadings," *Int. Jour. Impact Eng.* **30**, 385–401 (2004).
7. Knowles, J. K., "On shock waves in a special class of thermoelastic solids," *Int. Jour. Nonlinear Mechanics* **40**, 387–394 (2005).
8. Knowles, J. K., "Impact Induced Tensile Waves in a rubberlike material," *SIAM J. Appl. Math.* **62**(4), 1153–1175 (2002).
9. Abeyaratne, R., and Knowles, J. K., "On a shock-induced martensitic phase transition," *J. Appl. Phys.* **87**, 1123–1134 (2000).
10. Dai, H. H., and Kong, D. X., "The propagation of impact-induced tensile waves in a kind of phase transformation materials," *Jour. Comput. App. Math.* **190**, 57–73 (2006).
11. Chen, Y. C., and Lagoudas, D. C., "Impact induced phase transformation in shape memory alloys," *Journal of the Mechanics and Physics of Solids* **48**, 275–300 (2000).

12. Lagoudas, D. C., Ravi-Chandar, K., Sarh, K., and Popov, P., "Dynamic loading of polycrystalline shape memory alloy rods," *Mechanics of Materials* **35**, 689–716 (2003).

13. Bubner, N., "Landau-Ginzburg model for a deformation-driven experiment on shape memory alloys," *Continuum Mech. Thermodyn* **8**, 293–308 (1996).

14. Bubner, N., Mackin, G., and Rogers, R. C., "Rate dependence of hysteresis in one-dimensional phase transitions," *Comp. Mater. Sci.* **18**, 245–254 (2000).

15. Bales, G. S., and Gooding, R. J., "Interfacial dynamics at a 1st-order phase-transition involving strain dynamic twin formation," *Phys. Rev. Lett.* **67**, 3412 (1991).

16. Chaplygin, M. N., Darinskii, B. M., and Sidorkin, A. S., "Nonlinear waves in ferroelastics," *Ferroelectrics* **307**, 1–6 (2004).

17. Melnik, R. V. N., Robert, A. J., and Thomas, K. A., "Computing dynamics of copper-based SMA via central manifold reduction models," *Computational Material Science* **18**, 255–268 (2000).

18. Wang, L. X., and Melnik, R. V. N., "Numerical model for vibration damping resulting from the first order phase transformations," *Applied Mathematical Modeling* **31** 2008–2018 (2007).

19. Falk, F., "Driven domain walls in shape memory alloys," *J. Phys. C: Solid State Phys.* **20** 2501–2509 (1987).

20. Matus, P., Melnik, R. V. N., Wang, L. X., and Rybak, I., "Applications of fully conservative schemes in nonlinear thermoelasticity: Modelling shape memory materials," *Mathematics and Computers in Simulation* **65**(4–5) 489–509 (2004).

21. Niezgodka, M., and Sprekels, J., "Convergent numerical approximations of the thermomechanical phase transitions in shape memory alloys," *Numerische Mathematik* **58** 759–778 (1991).